ACADEMIA ROMÂNĂ
Revue Roumaine de Chimie
https://www.icf.ro/rrch/

Rev. Roum. Chim.,
2022, *67*(1-2), 63–70
DOI: 10.33224/rrch.2022.67.1-2.04

Dedicated to the memory of
Dr. Emilian GEORGESCU (1946-2020)

SOLID-STATE SYNTHESIS OF OPTIMIZED NASICON $Na_3Zr_2Si_2PO_{12}$ CERAMIC MEMBRANES

Adriana MARINOIU,* Mihaela IORDACHE and Athanasios TILIAKOS

National R&D Institute for Cryogenics & Isotopic Technologies, 4 Uzinei Street,
P.O. Box Râureni 7, 240050, Rm. Vâlcea, Roumania

Received September 29, 2021

We report on the solid-state reaction (SSR) synthesis protocols and post-synthesis processing parameters of NASICON $Na_3Zr_2Si_2PO_{12}$ ceramic membranes prepared from Na_2CO_3, SiO_2, ZrO_2, and $NH_4H_2PO_4$ precursors. Characterization was conducted by optical microscopy, granulometry (DLS), porosimetry (BET/ BJH), and X-ray diffractometry (XRD); electrical properties, i.e. electrical (dc) and ionic (ac) conductivity, were evaluated by impedance spectroscopic methods over the temperature range of 100°C to -100°C. Apart from NASICON composition, particular attention was focused on monitoring the role of post-synthesis processing parameters, *i.e.* sintering temperature and pellet-forming co ld isostatic pressure, on the derived electrical properties. In-lab prepared samples were compared with commercial NASICON pellets serving as reference for controlling the electrical properties. NASICON samples prepared by the SSR route at stoichiometric ratios of the precursors, sintered at 1100°C, and assembled into pellet form by cold-pressing at 3500 kgF, reached the same level of ionic conductivity as the commercial reference. This work serves as the initial step on our ongoing research into superionic ceramic conductors and their possible applications in energy conversion and storage.

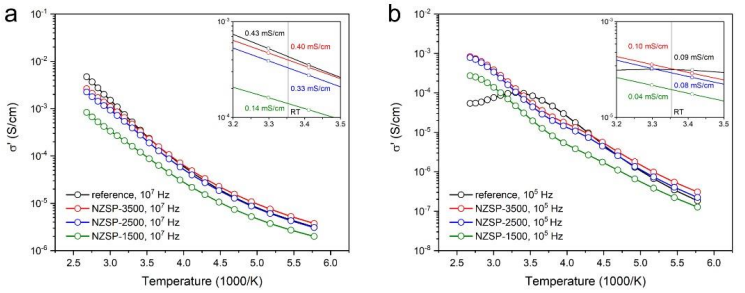

INTRODUCTION

An ongoing research quest spanning the entire 20th century, the history of solid ionic conductors can be traced back to 1932, with the identification of the different crystalline forms of alumina (common name of Al_2O_3 aluminium oxide, extracted from bauxite ore and used for the production of aluminium by smelting via Hall–Héroult electrolytic processes; the α form is generally known as the mineral corundum)[1]. However, the first promising break-through appeared much later in the late 1960s–early 1970s, with the measurement of sodium ion transport in β-alumina ($Na_2O{\cdot}11Al_2O_3$ with the general formula $Na_{1+x}Al_{11}O_{17+x/2}$; crystals develop during slow cooling of molten alumina assisted by the trace presence of Na_2O), due to a layered structure permitting ionic migration between successive planes.[2]

That initial success instigated renewed efforts to overcome the inherent limitations of β-alumina, leading to a new set of compounds named NASICON (Natrium Super Ionic Conductors) that comply with the general formula

* Corresponding author: adriana.marinoiu@icsi.ro

$Na_{1+x}Zr_2Si_xP_{3-x}O_{12}$ with $0 \leq x \leq 3$, displaying a 3D skeletal structure with tunnel size conducive to sodium ion migration.[3] The NASICON family can be expanded by the isovalent replacement of its Na, Zr, or Si basic units; in principle, it comprises a class of structurally isomorphous 3D-framework compounds with Na^+ ionic conductivities reaching the same scale as liquid electrolytes over elevated temperatures. The latter property motivated such diverse initial applications of the new ceramic materials as in ion-exchange membranes and sensors.[4] In view of the more recent mandates for locating suitable alternatives to costly lithium (both in terms of financial and environmental factors) in battery systems, the role of NASICON materials was reinvigorated as solid-state electrolytes for sodium-ion batteries due to the high abundancy, wide availability, and low cost of sodium.[5] Even more recent iterations have suggested using NASICON as solid electrolyte in seawater flow batteries, a new type of energy storage that seeks to take advantage of the hypothetically unlimited supply of the seawater flow electrolyte component for unparalleled scalability.[6]

Returning to the topic of NASICON synthesis, various methods have been developed over the years combining both chemical and physical routes, with the solid-state reaction (SSR) physicochemical method being dominant in the literature, followed by the sol-gel,Pechini,and chemical polymerization methods, as well as purely physical methods, such as laser and plasma depositions.[7] Concerning purely chemical synthesis methods, the sol-gel method has been described as economically advantageous, resulting in higher homogeneity and purity of the final product compared to other methods. However, the sol-gel procedure itself is precarious, requiring to cope with obstacles at each step of solution and gel preparations, as well as during the final heat treatment. On the other hand, chemical polymerization presents the advantage of forming NASICON compounds with the rhombohedral crystalline structure at room temperature, also eliminating the occurrence of "free-zirconia" contamination, consistently plaguing this class of solid electrolytes when formed by other methods. The method employs as precursors alkoxides of Na, Zr, Si, P and their substitutes, preferably having up to six carbons in the alkyl chain group, in liquid or solid form; typical alkoxide precursors include: $Na(OCH_3)$, $Na(OC_2H_5)$, $Na(OC_3H_7)$, $Zr(OC_3H_7)_4$, $Zr(OC_4H_9)_4$, $Si(OCH_3)_4$, $Si(OC_2H_5)_4$, $P(OC_3H7)_3$, etc. These are dissolved in an alcohol solvent, with some being partially hydrolyzed, and then mixed with polymerizing. The mechanism leading to oxide network formation requires the presence of two active groups in the polymer solutions: an ester (OR) group and a hydroxyl (OH) group. Total hydrolyzation of an alkoxide generally results in the formation of either inactive species, precipitated phase separation, or gelling. The above considerations, and the presumed complexity of having to deal with organometallically derived materials, condemned chemical polymerization to relative obscurity in favor of the more traditional SSR method.

As a general estimate, the reason for the dominance of the SSR method lies in its simplicity and versatility. Its precursors are employed strictly in solid state (e.g. Na_2CO_3, SiO_2, ZrO_2, and $NH_4H_2PO_4$), reacting via energetic ball or jet milling and forming the NASICON crystal structure by subsequent thermal processing. The method also allows for facile control of the chemical structure of the end material by precise manipulation of the stoichiometric ratios of constituents, and thus the selection between variations in the $Na_{1+x}Zr_2Si_xP_{3-x}O_{12}$ formula, e.g. setting x=2 for $Na_3Zr_2Si_2PO_{12}$ that represents the limit case for maximized ionic conductivity.[8] Such manipulations have produced numerous variations for optimizing the electrical properties of NASICON by controlling either the elemental composition (*e.g.* sodium content or alternative ions) or the grain boundaries within its crystalline lattice.[9] It should be noted here that such variations to the traditional SSR method also aim at minimizing or eliminating the contamination by monoclinic "free zirconia", occurring as an undesirable outcome of the high temperatures of thermal processing–especially over the final sintering stage at 1250°C.[7-9]

In our recent work, we conducted a series of experiments to investigate the classic $Na_3Zr_2Si_2PO_{12}$ system based on the SSR synthesis, where sintering temperatures were maintained at the highest level of 1250°C, thus not suppressing excess zirconia contamination, which was instead successfully controlled by manipulating the applied isostatic pressure during pellet formation.[10] Here, following the latest trends for lowering the final sintering temperature and incorporating our recent findings, we drop the temperature to the threshold of 1100°C to minimize zirconia contamination;[11] we then investigate the effects on

the material's crystalline structure and its ionic conductivity, using a commercially produced NASICON pellet as reference. The goal is to determine the validity and necessity of applying such highly elevated sintering temperatures, and if this can be circumvented by a suitable combination of processing parameters, i.e. calcination and sintering temperatures in conjunction with levels of applied isostatic pressure. For this reason, the traditional SSR protocol was followed for synthesizing the $Na_3Zr_2Si_2PO_{12}$ system, without controlling the elemental composition or the grain boundaries in the crystalline lattice.

RESULTS AND DISCUSSION

NASICON samples obtained during and after SSR synthesis, thermal processing, and pellet formation were analyzed by relevant methods to probe into the effects of the various processing stages on material properties. $Na_3Zr_2Si_2PO_{12}$ samples are referred to as NZSP-X, where X corresponds to the applied isostatic pressure [kgF] for pellet formation.

Optical images of the pre-sintering powder and post-sintering pellet samples are shown in **Figure 1**, as a first indicator of micro- and macrostructural effects. The microstructure of NASICON has been reported to have a major impact on its electrical properties, with sintering conditions being a major contributor to microstructural and macrostructural variations: ionic conductivity can be enhanced with sintering time due to an increase in grain growth and densification, up to a certain duration (40 h) after which the electrical performance is hindered due to the presence of a liquid phase along the grain boundaries.[10-12] The effects of aggregation on the macrostructure are displayed in the micrographs; cross-sections display visible anisotropy in the packing order as clusters of different orientations but with distinct grain boundaries; at sufficient pressures levels, high packing ratios of clusters and the structural integrity of pellets are achieved.[10]

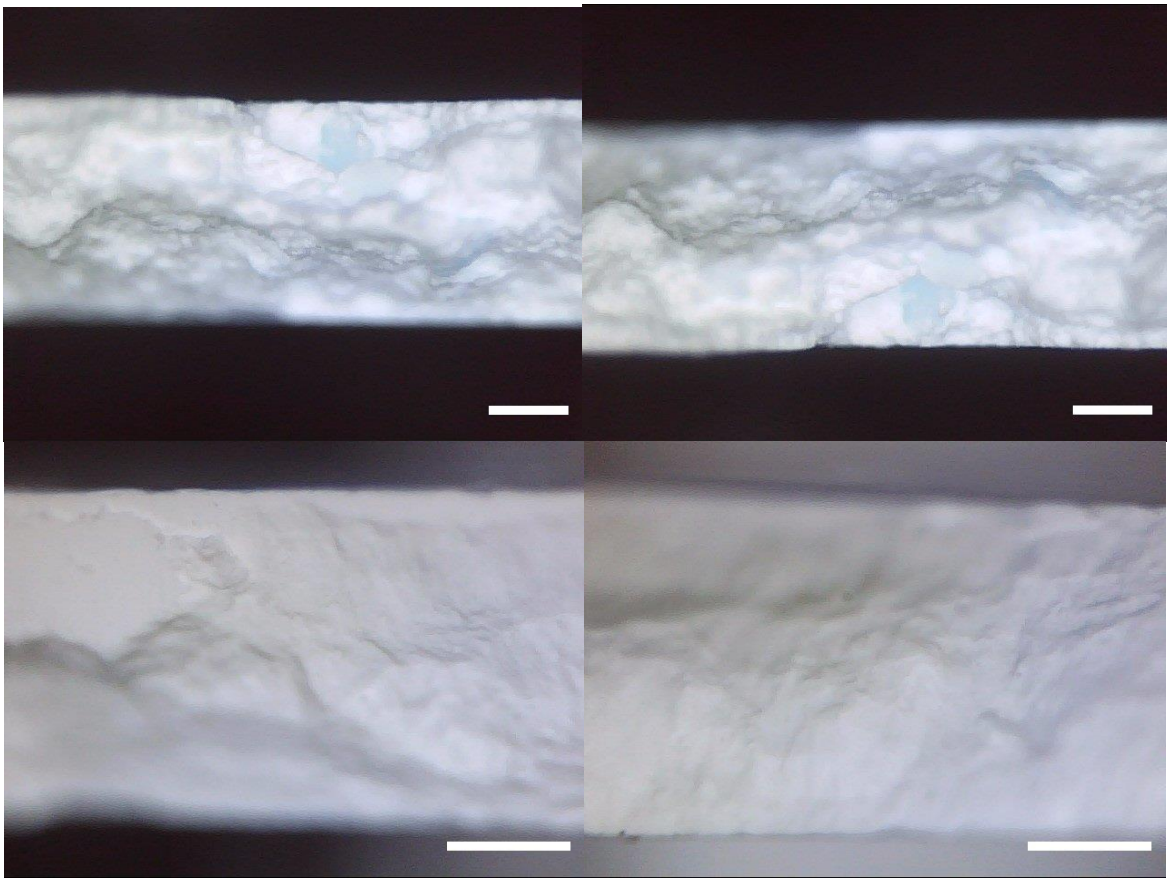

Fig. 1 – Optical microscopies of profiles views of NASICON pellets showing packing order of clusters at low applied pressure of 1500 kgF (*a*, *b*) and high pressure of 3500 kgF (*c*, *d*).

Table 1

Particle size distribution metrics of thermally untreated vs. treated NASICON samples

Sample	D_{10} [µm]	D_{50} [µm]	D_{90} [µm]	D_m [µm]
NZSP untreated	0.48	0.50	0.52	0.52
NZSP-1500	2.14	3.36	5.27	2.98
NZSP-2500	2.32	2.39	2.45	2.39
NZSP-3500	3.63	3.72	3.82	3.74

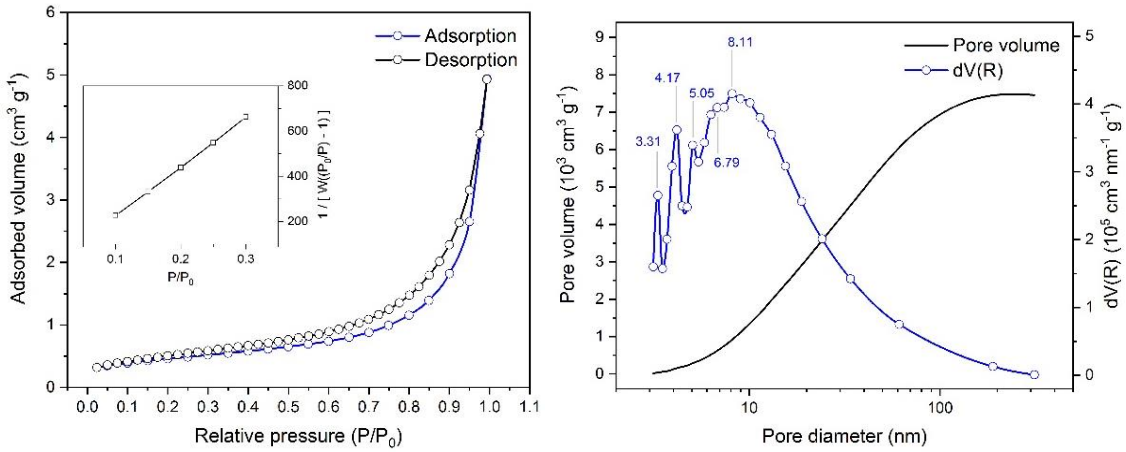

Fig. 2 – BET *(left)* and BJH *(right)* analysis of surface porosity for pre-sintering NASICON powders.

Particle size distributions of the pre-sintering and post-sintering NASICON materials, obtained by Dynamic Light Scattering (DLS) methods, determine the effectiveness of ball milling and thus the yield of SSR, while aggregation in the post-sintering material can affect its electrical properties due to clustering and percolation phenomena of zirconia contaminants through the NASICON lattice.[10] **Table 1** shows an overall submicronic size of the pre-sintering particles, which increases post-sintering due to aggregation. D_m corresponds to the modal diameter of the distributions, while D_A signifies the particle diameter corresponding to the cumulative distribution at A%. Analysis reveals that the sintered NASICON powders are polydisperse with an index above 70%, in contrast to the monodisperse pre-sintered material (effects of aggregation due to thermal processing), while both distributions are monomodal (modality is conserved before and after thermal processing, and refers to the effectiveness of ball milling).

Surface area estimation was conducted using BET/BJH analysis, based on nitrogen adsorption caused by intrinsic surface energies, and is presented in **Figure 2**. The pre-sintered powder registered a BET surface area of 1.6 $m^2\ g^{-1}$. The obtained adsorption/desorption isotherms indicate a hysteresis loop, suggesting the presence of mainly a mesoporous structure and a relatively poor porosity corresponding to IV-type isotherms.

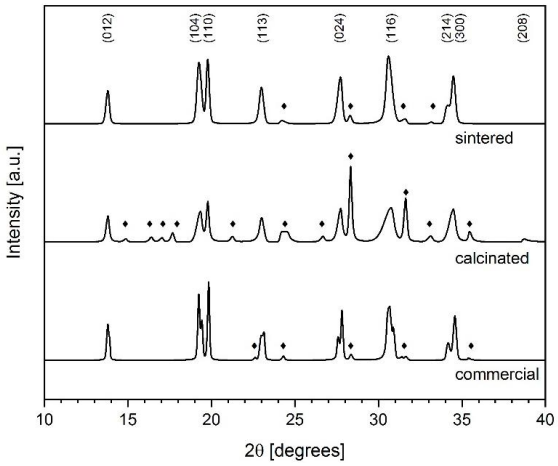

Fig. 3 – XRD spectra of NASICON samples before and after sintering, in comparison with the commercial control reference. Main NASICON peaks are identified according to their Miller indices; zirconia phases are marked by rhomboid symbols.

XRD diffractometry, presented in **Figure 3**, elucidated more on the microstructure of the prepared materials, after calcination and after the final sintering stage, in comparison to the commercial reference. Crystallographic Miller indices corresponding to primary NASICON signatures were obtained by comparison with the literature for NASICON materials of the same composition, with remaining peaks of smaller intensity corresponding to zirconia phases and/or impurities, according to COD cards 1529809 and

1530657 for NASICON (PDF 01-084-1190 and 00-035-0412), as well as COD 5000038 for zirconia (PDF 01-070-2491).[13] Detected signature peaks in sintered samples display high crystallinity for the primary NASICON phases. Interplanar *d* spacing distance is consistent with highly compacted phases, ranging from 0.6 to 0.1 nm in order of increasing 2θ angles, with the largest crystallite size registering less than 100 nm for the majority of phases. Partially formed NASICON phases are evident in pre-sintered (calcinated) samples, which also carry unreacted zirconia phases of virtually random orientations over smaller angles. For sintered samples, the primary NASICON peaks are restored and consistent with the spectra of the commercial control. After sintering, trace amounts of monoclinic ZrO_2 are observed, emerging due to P and Na volatilization from the main lattice during thermal treatment.

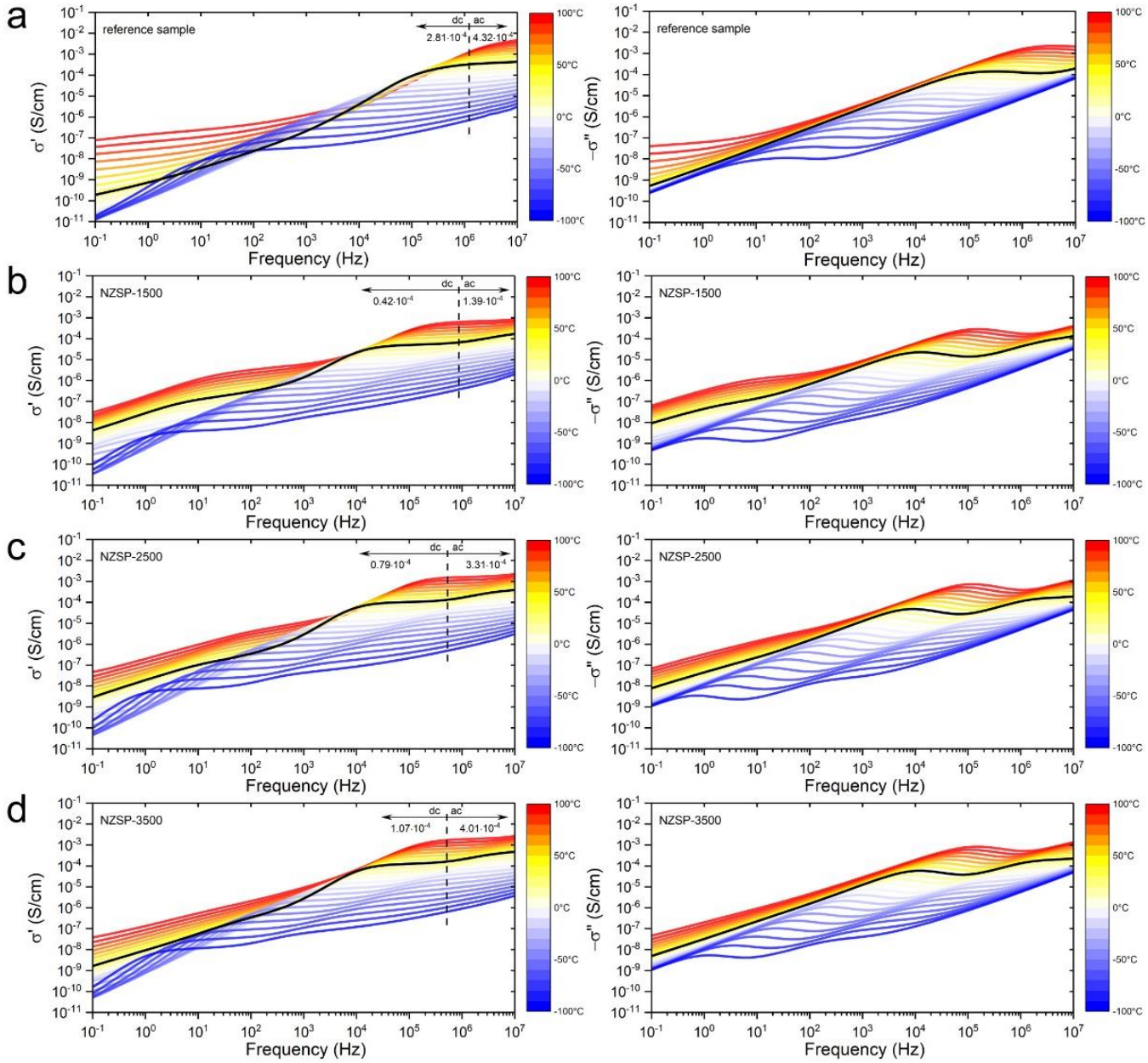

Fig. 4 – Real and imaginary conductivities, σ' and σ'' respectively, for the commercial reference *(a)*, and the in-lab prepared pellets NZP-1500 *(b)*, NZP-2500 *(c)*, and NZP-3500 *(d)*. Temperature profile colormaps are displayed on the right of figures; RT (25°C) scans are highlighted in bold.

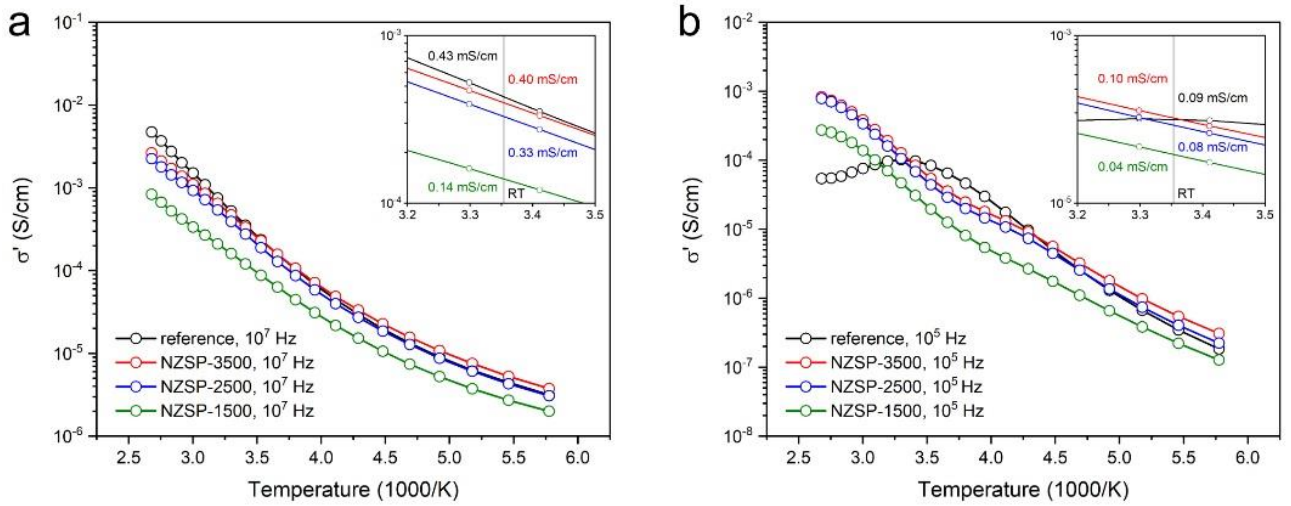

Fig. 5 – Arrhenius plots of the real conductivity *σ'* vs. reciprocal temperature for the 10^7 Hz dispersion region dominated by ac ionic conductivity *(a)*, and the 10^5 Hz plateau region dominated by dc conductivity *(b)*.

Concerning the key electrical properties of the synthesized materials, **Figure 4** shows the variation of the real and imaginary parts of conductivity, *σ'* and *σ''* respectively, against ac frequency over the temperature range of 100°C to -100°C, for NASICON pellets assembled over different isostatic pressure levels. The double-logarithmic plot of conductivity over frequency typically displays three regions classified based on frequency: *i*) the low-frequency polarization region; *ii*) the frequency-independent dc conductivity plateau; and *iii*) the high-frequency dispersive region corresponding to ac conductivity. The synthesized NASICON sample assembled at the highest pressure of 3500 kgF displayed electrical properties at the same scale as the reference, with ac conductivity climbing at 0.40 mS cm^{-1} vs. 0.43 mS cm^{-1} registered by the reference at the highest scanning frequency of 10^7 Hz at RT. Pellets formed at lower pressure levels displayed significantly lower ac conductivities, suggesting poor integrity of the NASICON lattice below a certain threshold of applied pressure. This diminishing trend is also displayed for dc conductivity, with the key difference of much lower values registered for the in-lab synthesized samples vs. the reference: for NZSP-3500 that displayed ac conductivity on par with the reference, its dc conductivity plateau settled at 0.11 mS cm^{-1} vs. 0.28 mS cm^{-1}. This observation suggests that lowering the final sintering temperature below 1250°C may compromise the integrity of the NASICON matrix by hindering the completion of the SSR process, affecting dc instead of ac conductivity. Finally, temperature dependency of the electrical properties is displayed as Arrhenius plots of the real conductivity *σ'* against scaled reciprocal temperature in **Figure 5**, manifesting as linear high-frequency regions that become distorted at lower frequencies due to polarization dominance. Overall, conductivity increases with temperature, with higher-temperature conduction being attributed to thermally activated polaron hopping and lower-temperature conduction being associated with bipolar hopping mechanisms.[10,14]

EXPERIMENTAL

$Na_3Zr_2Si_2PO_{12}$ synthesis was based on conventional solid-state reaction (SSR) protocols, using the following precursors in the stoichiometric ratio of 3:2:2:1 in terms of Na:Si:Zr:P (molar ratio of 1.5:2:2:1): Na_2CO_3 (98%, 0.5 mm particle size, Alfa Aesar), SiO_2 (0.7 mm particle size, Umicore), ZrO_2 (99%, 5 μm particle size, Sigma-Aldrich), and $NH_4H_2PO_4$ (0.5 mm particle size, Scharlab), without employing other fillers or additives. The precursors were mixed with ethanol solvent into a slurry, and processed for 9 h by ball milling (wet milling) using zirconia balls (10 mm, 5 mm, and 3 mm diameters) at 300 rpm in a sealed zirconia container, and then dried at 80°C. The powder was preheated at 600°C for 4 h, and then calcinated at 1100°C for 4 h in a N_2 gas flow to remove any volatile species. The calcinated powders were pulverized again for 2 h by wet milling at 500 rpm using 3 mm diameter balls. The obtained fine powders were pressed into pellets by cold isostatic pressing at 1500 kgF (NZSP-1500), 2500 kgF (NZSP-2500), and 3500 kgF (NZSP-3500) for 5 min, to form pellets of 16 mm diameter. These were transferred into a tubular furnace for sintering at 1100°C for 10 h in N_2 gas flux at the heating rate of 5°C min^{-1}. The reference NASICON membrane was purchased from 4TOONE Ltd., Korea.

Optical microscopies were collected on a portable electronic microscope. Pellet samples were broken along their diameters, so that images could be collected from cross-sectional profiles; powder samples were manually crushed in a mortar without the addition of solvent to retain crystalline formations.

Particle size distributions were obtained by Dynamic Light Scattering (DLS), conducted on a Nano DS Dual Light Scattering Particle Size Analyzer (CILAS), operated in Static Light Scattering (SLS) and in Dynamic (DLS) mode depending on the expected size range of the NASICON particles.

Surface area and microporosity analyses were performed on an Autosorb iQ analyzer (Quantachrome). Samples were degassed prior to analysis at 115°C for 4 to 6 hours; nitrogen adsorption/desorption isotherms were obtained at the temperature of 77 K. Specific surface areas were calculated according to the Brunauer-Emmett-Teller (BET) equation using the linearity criterion over the range of 0.1 to 0.3 P/P_0; the Barrett-Joyner-Halenda (BJH) equation was used to characterize pore size distributions based on desorption isotherms.

X-Ray Diffraction (XRD) measurements were conducted on a MiniFlex600 X-Ray diffractometer (RIGAKU) equipped with a CuK_a X-Ray source at the wavelength of 1.541838 Å. Scans were performed over the 10° to 40° range at high resolution (0.01° step, 1.0° min^{-1} scanning speed), using a monochromator to suppress background noise levels. NASICON samples were scanned in powder form as received, or were pulverized in a mortar when in pellet form.

Broadband conductivity measurements were performed on an Alpha-A Modular Measurement System from NOVOCONTROL for impedance spectroscopy, equipped with a Quattro Cryosystem temperature controller. Scans were performed over the frequency range of 0.1 Hz to 10 MHz and temperature range of 173 K to 393 K under a dry nitrogen atmosphere. Conductivity was measured isothermally in steps of 5 K using an AC voltage amplitude of 0.1 V. Prior to measurement, NASICON pellets were dried at 120°C for 2 h under N_2, and silver paint was administered on their surfaces to secure good contact with the measuring electrodes.

CONCLUSIONS

The classic $Na_3Zr_2Si_2PO_{12}$ system was investigated based on the solid-state reaction (SSR) synthesis method, with considerations for optimizing ac ionic conductivity, based on the selected processing parameters of sintering temperature and isostatic pressure. By keeping the temperature at the lower limit of 1100°C, zirconia contamination was mostly avoided, thus securing high ionic ac conductivity but having a detrimental effect on the secondary electrical dc conductivity. Investigating the effects of applied isostatic pressure for NASICON pellet formation, the maximum applied pressure of 3500 kgF produced the best results, with the in-lab prepared sample matching the ionic conductivity of the commercial reference, reaching 0.4 mS cm^{-2} at RT. Further experiments will investigate variations in the stoichiometry and their effect on the mechanical and electrical properties of NASICON.

Acknowledgements. The authors declare no conflict of interest regarding this work and would like to acknowledge Borța Simona, Iacob Ciprian, and Șișu Claudia of ICSI for providing additional measurements conducive to this project. The authors would like to acknowledge the financial support by the Ministry of Research, Innovation, and Digitization of Roumania through the National Plan of Research and Development, Project PN 19-11-02-01; and by the Executive Agency for Higher Education, Research, Development & Innovation Funding (UEFISCDI), through Project PN-III-P2-2.1-PED-2019-1894, Contract no. 460PED/2020.

REFERENCES

1. W. E. Haupin, *J. Chem. Educ.*, **1983**, *60*, 279–282; K. Grjotheim, H. Kvande and Q. Zhuxian, *JOM*, **1995**, *47*, 32–35; P. Mandin, R. Wüthrich and H. Roustan, *ECS Trans.*, **2009**, *19*, 1–10.
2. Y.-F. Yu Yao and J. T. Kummer, *J. Inorg. Nucl. Chem.*, **1967**, *29*, 2453–2475; M. S. Whittingham, *J. Chem. Phys.*, **1971**, *54*, 414–416; R. D. Armstrong, T. Dickinson and J. Turner, *Electrochim. Acta*, **1974**, *19*, 187–192; J. C. Wang, M. Gaffari and Sang-il Choi, *J. Chem. Phys.*, **1975**, *63*, 772–778; R. Stevens and J. G. P. Binner, *J. Mater. Sci.*, **1984**, *19*, 695–715.
3. H. Y.-P. Hong, *Mater. Res. Bull.*, **1976**, *11*, 173–182; J. B. Goodenough, H. Y-P. Hong and J. A. Kafalas, *Mater. Res. Bull.*, **1976**, *11*, 203–220; R. S. Gordon, G. R. Miller, B. J. McEntire, E. D. Beck and J. R. Rasmussen, *Solid State Ion.*, **1981**, *3*, 243–248; H. Kohler and H. Schulz, *Solid State Ion.*, **1983**, *9*, 795–798; H. Kohler, H. Schulz and O. Melnikov, *Mater. Res. Bull.*, **1983**, *18*, 1143–1152; V. A. Nicholas, P. J. Johnson and A. I. Kingon, *Solid State Ion.*, **1985**, *17*, 351–357; H. Kohler and H. Schulz, *Mater. Res. Bull.*, **1985**, *20*, 1461–1471; H. Kohler and H. Schulz, *Mater. Res. Bull.*, **1986**, *21*, 23–31; K. D. Kreuer, H. Kohler, U. Warhus and H. Schulz, *Mater. Res. Bull.*, **1986**, *21*, 149–159; K. D. Kreuer and U. Warhus, *Mater. Res. Bull.*, **1986**, *21*, 357–363.
4. Y. Saito and T. Maruyama, *Solid State Ion.*, **1988**, *28*, 1644–1647; Y. Sheng, S. Youichi, M. Norio and Y. Noboru, *Chem. Lett.*, **1990**, *19*, 2033–2036; B. E. Scheetz, D. K. Agrawal, E. Breval and R. Roy, *Waste Manage.*, **1994**, *14*, 489–505; S. Balagopal, T. Landro, S. Zecevic, D. Sutija. S. Elangovan and A. Khandkar, *Sep. Purif. Technol.*, **1999**, *15*, 231–237.
5. Y. Noguchi, E. Kobayashi, L. S. Plashnitsa, S. Okada and J. Yamaki, *Electrochim. Acta*, **2013**, *101*, 59–65; F. Lalère, J. B. Leriche, M. Courty, S. Boulineau, V. Viallet, C. Masquelier and V. Seznec, *J. Power Sources*, **2014**, *247*, 975–980; G. Crabtree, E. Kócs and L. Trahey, *MRS Bull.*, **2015**, *40*, 1067–1078; M. Guin and F. Tietz, *J. Power Sources*, **2015**, *273*, 1056–1064; M. Guin, F. Tietz and O. Guillon, *Solid State Ion.*, **2016**, *293*, 18–26; C. Zhao, L. Liu, X. Qi, Y. Lu, F. Wu, J. Zhao, Y. Yu, Y.-S. Hu and L. Chen, *Adv. Energy Mater.*, **2018**, *8*, 1703012; Y. Ruan, F. Guo, J. Liu, S. Song, N. Jiang and B. Cheng, *Ceram. Int.*, **2019**, *45*, 1770–1776; Y. Wang, S. Song, C. Xu, N. Hu, J. Molenda and L. Lu, *Nano Mater. Sci.*, **2019**, *1*, 91–100.
6. J.-K. Kim, E. Lee, H. Kim, C. Johnson, J. Cho and Y. Kim, *Chem. Electro. Chem.*, **2015**, *2*, 328–332; *Electrochim. Acta*, **2016**, *191*, 1–7; H. Bae, J.-S. Park, S. T. Senthilkumar, S. M. Hwang and Y. Kim, *J. Power Sources*, **2019**, *410*, 99–105; S. M. Hwang, J.-S. Park, Y. Kim, W. Go, J. Han, Y. Kim and Y. Kim, *Adv. Mater.*, **2019**, *31*, 1804936.

7. B. E. Yoldas and I. K. Lloyd, *Mat. Res. Bull.*, **1983**, *18*, 1171–1177; M. Meunier, R. Izquierdo, L. Hasnaoui, E. Quenneville, D. Ivanov, F. Girard, F. Morin, A. Yelon and M. Paleologou, *Appl. Surf. Sci.*, **1998**, *127*, 466–470; A. Ignaszak, P. Pasierb, R. Gajerski and S. Komornicki, *Thermochim. Acta*, **2005**, *426*, 7–14; F. Ejehi, S. P. H. Marashi, M. R. Ghaani and D. F. Haghshenas, *Ceram. Int.*, **2012**, *38*, 6857–6863; M. Pérez-Estébaneza, J. Isasi-Marín, A. Rivera-Calzada, C. León and M. Nygren, *J. Alloy. Compd.*, **2015**, *651*, 636–642; S. Naqash, Q. Ma, F. Tietz and O. Guillon, *Solid State Ion.*, **2017**, *302*, 83–91; S. A. Novikova, R. V. Larkovich, A. A. Chekannikov, T. L. Kulova, A. M. Skundin and A. B. Yaroslavtsev, *Inorg. Mater.*, **2018**, *54*, 794–804.
8. O. Bohnke, S. Ronchetti and D. Mazza, *Solid State Ion.*, **1999**, *122*, 127–136; R. O. Fuentes, F. M. Figueiredo, F. M. B. Marques and J. I. Franco, *Solid State Ion.*, **2001**, *140*, 173–179; J. W. Fergus, *Solid State Ion.*, **2012**, *227*, 102–112.
9. N. S. Bell, C. Edney, J. S. Wheeler, D. Ingersoll and E. D. Spoerke, *J. Am. Ceram. Soc.*, **2014**, *97*, 3744–3748; H. Park, K. Jung, M. Nezafati, C.-S. Kim and B. Kang, *ACS Appl. Mater. Interfaces*, **2016**, *8*, 27814–27824; M. Samiee, B. Radhakrishnan, Z. Rice, Z. Deng, Y. S. Meng, S. P. Ong and J. Luo, *J. Power Sources*, **2017**, *347*, 229–237; H. Park, M. Kang, Y. C. Park, K. Jung and B. Kang, *J. Power Sources* **2018**, *399*, 329–336; K. Suzuki, K. Noi, A. Hayashi and M. Tatsumisago, *Scr. Mater.*, **2018**, *145*, 67–70; S. Naqash, F. Tietz, E. Yazhenskikh, M. Müller and O. Guillon, *Solid State Ion.*, **2019**, *336*, 57–66.
10. A. Tiliakos, M. Iordache and A. Marinoiu, *Appl. Sci.*, **2021**, *11*, 8432.
11. A. Jalalian-Khakshour, C. O. Phillips, L. Jackson, T. O. Dunlop, S. Margadonna and D. Deganello, *J. Mater. Sci.*, **2020**, *55*, 2291–2302; C. S. Martínez-Cisneros, B. Pandit, C. Antonelli, J. Y. Sanchez, B. Levenfeld and A. Varez, *J. Eur. Ceram. Soc.*, **2021**, *41*, 7723–7733; B. Santhoshkumar, D. L. R. Khanna, M. B. Choudhary, P. L. Rao, K. V. Ramanathan, A. K. Bera, S. M. Yusuf and B. Pahari, *Chem. Phys. Let.*, **2021**, *776*, 138706; Y. Xing, Y. Li and C. Zhang, *Solid State Ion.*, **2021**, *373*, 115811; J. A. S. Oha, Y. Wanga, Q. Zeng, J. Sun, Q. Sun, M. Goh, B. Chua, K. Zeng and L. Lu, *J. Colloid Interface Sci.*, **2021**, *601*, 418–426; F. Sun, Y. Xiang, Q. Sun, G. Zhong, M. N. Banis, W. Li, Y. Liu, J. Luo, R. Li, R.Fu, T.-K. Sham, Y. Yang, X. Sun and X. Sun, *ACS Appl. Mater. Interfaces*, **2021**, *13*, 13132−13138.
12. T. Zangina, J. Hassan, K. A. Matori, R. S. Azis, U. Ahmadu and A. See, *Results Phys.*, **2016**, *6*, 719–725; J. A. Oh, L. He, A. Plewa, M. Morita, Y. Zhao, T. Sakamoto, X. Song, W. Zhai, K. Zeng and L. Lu, *ACS Appl. Mater. Interfaces*, **2019**, *11*, 40125–40133; S. Narayanan, S. Reid, S. Butler and V. Thangadurai, *Solid State Ion.*, **2019**, *331*, 22–29; A. Jalalian-Khakshour, C. O. Phillips, L. Jackson, T. O. Dunlop, S. Margadonna and D. Deganello, *J. Mater. Sci.*, **2020**, *55*, 2291–2302.
13. J. J. Didisheim, E. Prince and B. J. Wuensch, *Solid State Ion.*, **1986**, *18*, 944–958; P. R. Rudolf, A. Clearfield and J. D. Jorgensen, *J. Solid State Chem.*, **1988**, *72*, 100–112; U. Martin, H. Boysen and F. Frey, *Acta Crystallogr. B Struct. Sci. Cryst.*, **1993**, *49*, 403–413; A. G. Jolley, D. D. Taylor and N. J. Schreiber, *J. Am. Ceram. Soc.*, **2015**, *98*, 2902–2907.
14. D. P. Almond, G. K. Duncan and A. R. West, *Solid State Ion.*, **1983**, *8*, 159–164; G. Govindaraj and C. R. Mariappan, *Solid State Ion.*, **2002**, *147*, 49–59; C. R. Mariappan and G. Govindaraj, *Mater. Sci. Eng. B*, **2002**, *94*, 82–88; T. B. Schrøder and J. C. Dyre, *Phys. Rev. Lett.*, **2008**, *101*, 025901; S. Mudenda and G. M. Kale, *J. Mater. Chem. A*, **2015**, *3*, 12268–12275.